Validation of the CERES/TRMM ERBE-Like Monthly Mean Clear-Sky Longwave Dataset and the Effects of the 1998 ENSO Event

TAKMENG WONG AND DAVID F. YOUNG

NASA Langley Research Center, Hampton, Virginia

MARTIAL HAEFFELIN AND STEPHANIE WECKMANN

Virginia Polytechnic Institute and State University, Blacksburg, Virginia

(Manuscript received 7 June 1999, in final form 27 December 1999)

ABSTRACT

The Clouds and the Earth's Radiant Energy System (CERES) is a new National Aeronautics and Space Administration space-borne measurement project for monitoring the radiation environment of the earth–atmosphere system. The first CERES instrument was launched into space on board the Tropical Rainfall Measuring Mission (TRMM) satellite on 27 November 1997. The purpose of this paper is 1) to describe the initial validation of the new CERES/TRMM Earth Radiation Budget Experiment (ERBE)–like monthly mean clear-sky longwave (CLW) dataset and 2) to demonstrate the scientific benefit of this new dataset through a data application study on the 1998 El Niño–Southern Oscillation (ENSO) episode. The initial validation of the CERES CLW data is carried out based on comparisons with both historical ERBE observations and radiative transfer simulations. While the observed CERES CLWs are initially larger than the historical ERBE record during the first part of the 1998 ENSO event, these differences are diminished by the end of the ENSO event in July 1998. These unique ENSO-related CLW radiation signatures are captured well by the radiative transfer model simulations. These results demonstrate that the new CERES CLW fluxes are theoretically consistent with the underlying physics of the atmosphere. A CERES data application study is performed to examine the relationship between the CERES CLW anomaly and changes in sea surface temperature (SST) and atmospheric column precipitable water content (PWC) during the January 1998 ENSO event. While the changes in the SST pattern are basically uncorrelated with changes in the CLW field, a negative correlation is found between the PWC anomaly and the changes in the CLW radiation field. These observed features point to 1) the significant role of the water vapor field in modulating the tropical outgoing CLW radiation field during the 1998 ENSO event and 2) the important effects of water vapor absorption in decoupling the top of the atmosphere tropical outgoing CLW radiation from the surface upward CLW field.

1. Introduction

Continuous monitoring of the earth's radiation field at the top of the atmosphere (TOA) is essential for understanding natural and anthropogenic-induced changes to the earth's climate. To achieve this important science goal, the National Aeronautics and Space Administration (NASA) has begun the Clouds and the Earth's Radiant Energy System (CERES) project (Wielicki et al. 1995, 1996), which consists of earth radiation budget instrument packages flying on three different satellites beginning with the Tropical Rainfall Measuring Mission (TRMM) satellite (Simpson et al. 1988) on 27 November 1997. The other CERES instruments are scheduled for Terra, which is previously known as the EOS-AM1 (Earth Observing System, 1030 LT sun-synchronous orbit) satellite, in December 1999 and the EOS-PM1 (1330 LT sun-synchronous orbit) satellite in December 2000. Building on the successful Earth Radiation Budget Experiment (ERBE) project (Barkstrom 1984; Barkstrom et al. 1989), this multisatellite Earth Radiation Budget (ERB) mission will provide the scientific community with necessary information for monitoring and understanding the earth's radiation environment well into the next century.

In order to accommodate both the scientific needs for maintaining a long-term consistent ERB dataset for monitoring long-term climate change and the desires for improving the accuracy over the previous climate datasets, the CERES science team has decided early in the mission to produce two different sets of TOA monthly mean data products to satisfy these requirements. These two datasets are the CERES ERBE-like monthly mean TOA data product and the CERES enhanced monthly mean TOA dataset (Wielicki et al. 1998). The main

Corresponding author address: Dr. Takmeng Wong, NASA Langley Research Center, MS 420, Hampton, VA 23681-2199.
E-mail: takmeng.wong@larc.nasa.gov

purpose of the former CERES data product is to provide continuity with the historical ERBE data record. Therefore, the CERES ERBE-like data system is based on the same processing system that was used by the ERBE experiment in an effort to ensure consistency between the two ERB products. The processing system includes the same ERBE angular distribution models (ADMs; Suttles et al. 1988), scene identification technique (Wielicki and Green 1989), time–space averaging algorithm (Brooks et al. 1986; Young et al. 1998), and output data structures. The latter CERES data product is an advanced radiation dataset that will provide a set of more accurate monthly mean TOA fluxes than those offered by the CERES ERBE-like product. The CERES enhanced monthly mean TOA dataset uses additional information from the onboard cloud imager for improved scene identification process (Wielicki et al. 1996). It also incorporates advanced diurnal modeling techniques through the introduction of geostationary satellite radiances (Young et al. 1998). In accordance with the new NASA/EOS data policy, these new CERES monthly mean TOA data products are scheduled to be archived at the Langley Distributed Active Archive Center (DAAC) as soon as they are validated. In order to provide the highest quality datasets to the scientific community and to maximize available validation resources, the CERES science team has decided to certify the CERES data in a stepwise fashion. The initial validation effort will concentrate on the ERBE-like dataset and release the TOA monthly mean data product within the first year after the launch of each satellite. The CERES enhanced TOA monthly mean dataset, on the other hand, will be released for archives at a later date (currently at 42 months after launch) to allow the CERES science team to conduct detailed validation studies on this new dataset.

The first CERES instrument was successfully launched into orbit on the TRMM satellite during the 1997/98 El Niño–Southern Oscillation (ENSO) event. Following a month of initial instrument monitoring and testing, production of the instantaneous CERES/TRMM ERBE-like data started in January 1998 and the first monthly mean CERES/TRMM ERBE-like data were delivered to the CERES science team for examination in February 1998. The validation of the ERBE-like instantaneous fluxes have been performed and their results are presented in the data quality summary documentation for the CERES/TRMM ERBE-like instantaneous data product. Readers are referred to the CERES/TRMM ERBE-like instantaneous data quality summary Web site (http://eosweb.larc.nasa.gov/PRODOCS/ceres/ES8/Quality_Summaries) at the Langley DAAC for more details. After 9 months of initial intensive postlaunch validation, the CERES/TRMM edition-1 ERBE-like dataset was approved by the CERES science team and released to the scientific community in October 1998. The goal of this paper is 1) to describe the initial postlaunch validation for the clear-sky longwave component of the CERES/TRMM edition-1 ERBE-like monthly mean data product [hereafter referred to as ERBE-like clear-sky longwave (CLW)] and 2) to demonstrate the scientific benefit of this new dataset through a CERES data application study on the 1998 ENSO episode. Section 2 outlines the scientific approach used in the postlaunch validation of the ERBE-like CLW data. Section 3 presents a description of the postlaunch validation datasets, including both the clear-sky radiation and the meteorological data, and a brief overview of the radiative transfer model. The results for the ERBE-like CLW postlaunch validation and the initial ERBE-like CLW data application study on the 1998 ENSO event are given in sections 4 and 5, respectively. Section 6 delivers the final summary and conclusion.

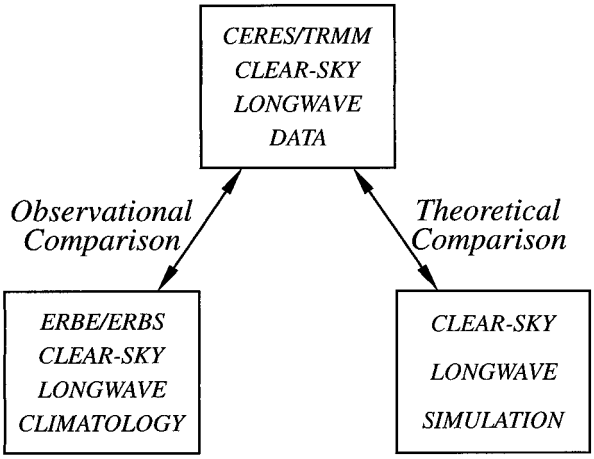

FIG. 1. Validation diagram for the CERES/TRMM ERBE-like clear-sky longwave flux showing both the observational and theoretical comparison processes.

2. Postlaunch validation approach

The CERES science team adopted a systematic approach for certifying the CERES data products. The postlaunch validation of the ERBE-like CLW dataset is carried out through a two-step process study of observational and theoretical analyses as shown in Fig. 1. The first step involves comparing temporal and spatial averages of the new ERBE-like CLW data with the historical ERBE CLW records. Special emphasis is placed on examining CLW data over the tropical ocean regions 30°N–30°S latitude. Since the new ERBE-like CLW data were collected during one of the largest ENSO events in the twentieth century, the CERES science team fully expects to see significant differences between these two data records due to changes in underlying surface and atmospheric conditions. Once the observational analyses are accomplished, the second step in the postlaunch validation process is to examine the consistency of the observed CLW with radiative transfer theory through comparisons with model simulations. Radiative transfer simulations for CLW over tropical oceanic regions 30°N–30°S are performed. The simulated results are

compared directly with CERES ERBE-like observations to determine theoretical coherence of this dataset with the underlying atmospheric and surface conditions of the earth–atmosphere system.

3. Postlaunch validation datasets

a. Broadband clear-sky longwave radiation datasets

Broadband clear-sky longwave radiation data from the historical ERBE record are used in the postlaunch validation of the CERES/TRMM ERBE-like edition-1 dataset in order to assess the differences and/or similarities between the two ERB datasets. This dataset consists of 5 yr of Earth Radiation Budget Satellite (ERBS) scanner S-4G monthly mean data from the ERBE experiment. The 5 yr of ERBE data are from January 1985 to December 1989. The ERBE S-4G dataset contains regional 2.5° grid boxes of monthly mean TOA emitted longwave and reflected shortwave radiation for total-sky and clear-sky conditions. For this validation study, only regional monthly mean clear-sky longwave radiation data over the tropical oceanic regions between 30°N and 30°S latitude are extracted from the ERBE/ERBS S-4G data product for analysis. The first 7 months of the 1998 ERBE-like data from the CERES/TRMM edition-1 ES-4G dataset are also used for the postlaunch validation. The CERES ES-4G dataset is organized in a similar fashion as the ERBE S-4G dataset and contains regional 2.5° grid boxes of monthly mean TOA emitted longwave and reflected shortwave radiation for total-sky and clear-sky conditions. For the comparative study, regional monthly mean clear-sky longwave radiation data over the tropical oceans are extracted from the CERES/TRMM edition-1 ES-4G data product. Clear-sky data from the ERBE/*ERBS* S-4G data product are used to construct climatological mean fields as well as other statistical information about the historical dataset. In addition, the 1998 CLW ENSO anomaly field (defined as the CERES/TRMM ERBE-like CLW flux minus the climatological mean CLW value from the historical ERBE/*ERBS* period) is computed to estimate the magnitude of the 1998 ENSO event.

The monthly mean uncertainties in calibration stability, angle sampling, time–space sampling for the CERES/TRMM edition-1 ERBE-like tropical mean longwave data between 20°N and 20°S latitude are estimated to be on the order of 0.6, 0.25, and 0.2 W m^{-2}, respectively. For the ERBE/ERBS dataset, the uncertainty due to calibration stability is on the order of 1.2 W m^{-2}. Uncertainties in angle sampling and time–space sampling for ERBE/ERBS data are the same as the CERES/TRMM edition-1 ERBE-like dataset. In addition to these uncertainties, both the CERES/TRMM edition-1 ERBE-like monthly mean CLW data and the ERBE/*ERBS* monthly mean CLW data also contain the same uncertainty due to the ERBE scene identification method used in defining the clear-sky scene in the observations (Harrison et al. 1990; Hartmann and Doelling 1991; Hartmann et al. 1992; Ockert-Bell and Hartmann 1992; Kiehl and Briegleb 1992). This uncertainty in clear-sky scene identification can lead to an overestimation of clear-sky longwave flux by as much as 3–4 W m^{-2} in both datasets.

b. Meteorological and surface datasets

The meteorological and surface datasets used in this study come from the National Oceanic and Atmospheric Administration (NOAA) Reynolds sea surface temperature (SST) dataset and a subset (temperature and moisture) of the NOAA/National Centers for Environmental Prediction (NCEP) dataset. Data corresponding to the historical ERBE period and the first 7 months of 1998 are obtained for use in the radiative transfer simulations. These data consist of two-dimensional distributions of SST, vertical column integrated atmospheric precipitable water content (PWC), and three-dimensional temperature and moisture profiles of the atmosphere. The three-dimensional atmospheric dataset includes both temperature information at 17 atmospheric pressure levels between 1000 and 30 mb and moisture information at the lowest 8 atmospheric pressure levels between 1000 and 300 mb. Moisture information between 300- and 30-mb pressure levels is not available from the NOAA/NCEP dataset. Climatological mean and anomalies (defined as the field value from CERES period minus the climatological mean value from the historical ERBE period) of SST and PWC for the tropical ocean within 30°N–30°S latitude are computed from these datasets for further analyses with the observed clear-sky longwave radiation field.

c. Radiative transfer simulation dataset

The radiative transfer model used to simulate the observed tropical oceanic TOA clear-sky longwave fluxes in this study is the Fu–Liou plane-parallel, delta-four-stream model (Fu and Liou 1993). This model has been tested extensively against both line-by-line calculations using idealized climatological test conditions and observations from intensive field experiments over the Department of Energy Atmospheric Radiation Measurement site in Oklahoma (Charlock and Alberta 1996). For example, the TOA CLW difference between the line-by-line calculations and the Fu–Liou model for a standard McClatchey tropical atmosphere (McClatchey et al. 1972) is found to be less than -0.5 W m^{-2}. The Fu–Liou model will also be used in the CERES operational data processing system for computing CERES atmospheric and surface flux products (Charlock et al. 1995). The clear-sky longwave part of this model uses a correlated-k treatment (Fu and Liou 1992) of gaseous absorption and emission for H_2O, CO_2, O_3, O_2, CH_4, and N_2O. The effect of chlorofluorocarbons is not included in this model and this may add a $+0.4$ W m^{-2}

uncertainty in the model calculation for a McClatchey tropical atmosphere. Twelve spectral intervals are used in the longwave part of the spectrum (2200–1 cm^{-1}). Continuum absorption of H_2O is also included (280–1250 cm^{-1}) using Clough–Kneizys–Davies (CKD) version 2.1 continuum. Comparing with the latest version of CKD continuum (version 2.3), the current model will produce a -1.1 W m^{-2} uncertainty in the TOA CLW for the McClatchey tropical atmosphere. For this study, the uniform mixing ratios for CO_2, CH_4, and N_2O are 350, 1.6, and 0.28 ppmv, respectively. Ozone profile is taken from the McClatchey tropical atmosphere. Other inputs to this model include NOAA Reynolds SST and the thermodynamical subset of the NOAA/NCEP atmospheric datasets. In addition, McClatchey tropical atmospheric moisture information is used to uniformly fill in the missing NOAA/NCEP upper-level moisture profile above the 300-mb pressure level. In order to assess the model uncertainty due to changes in upper-tropospheric humidity (UTH), a set of calculations are performed using standard McClatchey tropical atmosphere. The results of these calculations suggest that a 50%/100% decrease in UTH can cause an additional increase of 3.9–15.68 W m^{-2} to the TOA CLW, respectively. With these uncertainties in mind, CLW simulations are performed for the first 7 months of 1998 and for the corresponding ERBE period. In addition, theoretical CLW ENSO anomalies (defined as the CERES simulation minus the climatological mean value from the historical ERBE simulations) are also constructed from these modeled CLW data to facilitate comparison with observations.

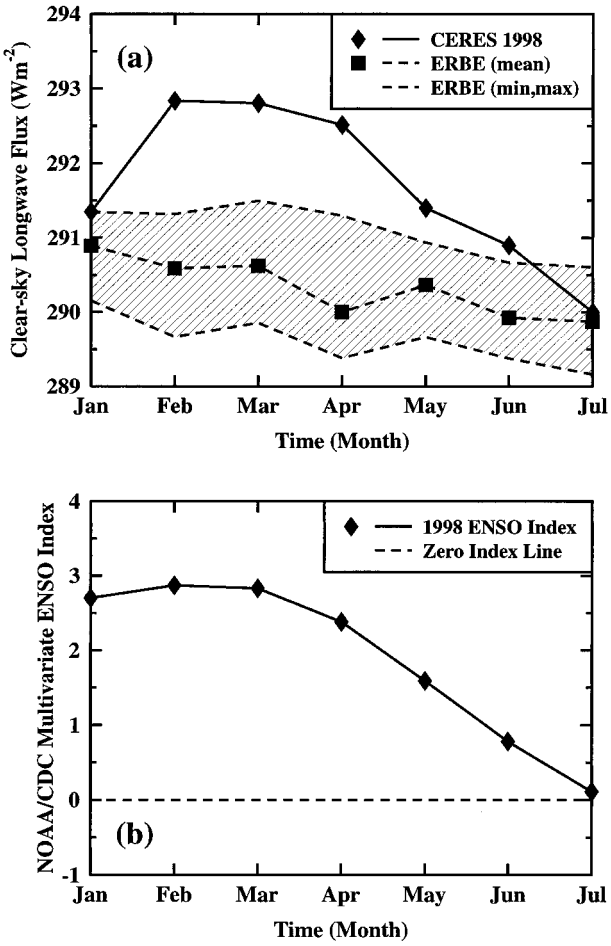

FIG. 2. Time series of (a) the CERES/TRMM ERBE-like clear-sky longwave oceanic tropical mean value (diamonds) for the first 7 months of 1998 and their corresponding ERBE climatological mean (squares) and range values (shaded area) during the first 7 months of the calendar year and (b) NOAA/CDC multivariate ENSO index value for the same period of 1998.

4. Postlaunch validation results

a. Observational analyses

This section will examine the observed CERES ERBE-like CLW flux and its relationship to the historical ERBE data. First, oceanic CLW tropical mean (defined as the CLW flux over tropical oceanic regions between 20°N and 20°S latitude) is used to assess the temporal behavior of the ERBE-like CLW data and their association with the historical ERBE data during the first 7 months of 1998. Next, regional analyses of the CLW and CLW anomaly field at the peak of the ENSO event are used to further highlight specific differences between these observations. The information gathered from these observational analyses will be used as the basis for comparison with theoretical simulations in the next section.

1) TEMPORAL VARIATIONS OF CLW

Figure 2a shows the time series of the CERES ERBE-like oceanic CLW tropical mean flux (given by diamond symbol and solid line) during the first 7 months of 1998. Superimposed on this figure is the corresponding climatology from the 5 yr of ERBE data. The climatological monthly mean and extreme values are represented in the figure by the square symbol and the shaded area, respectively. Figure 2b gives the corresponding time series of the NOAA Climate Diagnostic Center (CDC) multivariate ENSO index value (Wolter and Timlin 1993, 1998) for the same period. This index is based on six main observed variables over the tropical Pacific Ocean including sea level pressure, zonal and meridional surface wind, sea surface temperature, surface air temperature, and total cloud fraction. The zero ENSO index line is also given in the figure for reference. Two features are evident from inspection of these figures. First, an ENSO-like behavior in the CLW tropical mean is found in the CERES ERBE-like data. The temporal CLW fluctuation in Fig. 2a is well correlated with the time variation of NOAA multivariate ENSO index in Fig. 2b. This provides the first direct link between the observed behavior of the CLW energy field and the

evolution of the 1998 ENSO event. The CLW time series shows a dramatic increase between January and February 1998. At the same time, the NOAA multivariate ENSO index only shows a small corresponding increase in the index value. Since the multivariate ENSO index in December 1997 (not shown) was one-half point lower than the January 1998 value, the large change between January and February CERES oceanic CLW tropical mean is perhaps a delayed response between the NOAA multivariate ENSO index and the CERES oceanic CLW tropical mean value. After reaching a maximum value of 292.9 W m^{-2} in February, the CLW tropical mean remains at this level in March. It begins to take a large downward turn in April and reaches its minimum value of 290 W m^{-2} in July 1998. The NOAA multivariate ENSO index in Fig. 2b shows a similar temporal behavior and reaches a near-zero value in July. A zero ENSO index value represents the return to the mean climatological condition and the end of the 1998 ENSO event. Second, the CERES ERBE-like tropical mean is much larger than the ERBE climatology during most of this ENSO period. These differences, however, diminish completely by the end of the ENSO event in July 1998. The largest CLW differences between the CERES ERBE-like and the ERBE record for 1998 is 2.6 W m^{-2}. A temporal sampling error analysis was performed using hourly Geostationary Operational Environmental Satellite (GOES) data subsampled using simulated TRMM and ERBS orbital passes and then compared to the full 24-h dataset (Young et al. 1998). The analysis determined the uncertainty in LW tropical mean fluxes expected for CERES ERBE-like data on TRMM and for the ERBE data using the ERBS precessing orbit data. TRMM precesses through all local hours at the equator every 23 days, and ERBS does the same in 36 days. For 20°N–20°S, the GOES simulation indicate 1-sigma uncertainties of 0.2 W m^{-2} for both ERBE/ERBS and CERES/TRMM. The observed positive 2.6 W m^{-2} difference in the CLW tropical mean is much larger than the temporal sampling bias associated with the orbital differences between the TRMM and the ERBS spacecrafts and is indicative of the warming effect caused by the 1998 ENSO event over the tropical oceans.

2) Regional analysis of the CLW and CLW anomaly fields

In order to examine in more detail the observed regional differences between the CERES ERBE-like and the ERBE CLW data, a spatial analysis was performed for February 1998, corresponding to the peak of the 1998 ENSO event, over tropical oceans within latitude 30°N and 30°S. Figures 3a and 3b show the spatial features of the CERES ERBE-like CLW distribution and the CLW anomaly (or differences) with respect to the historical ERBE period over tropical oceans during February 1998. Overall, the CLW radiation over tropical oceans for this month has values from 271 to 309 W m^{-2}. Three large-scale zonal features are apparent in this figure: 1) a zone of maximum CLW radiation centered near 10°–15°N, 2) a zone of minimum energy at the equatorial region, and 3) a zone of secondary maximum radiation centered near 10°–15°S. The warmest oceanic area is found just west of the international date line in the Northern Hemisphere. While the CLW distribution over the Northern Hemisphere is dominated by a large continuous zone of high-CLW radiation, the CLW pattern in the Southern Hemisphere is less continuous. Regions of high-CLW radiation are found to the west of all the major continents in the Southern Hemisphere. The zone of equatorial minimum CLW energy is quite continuous and extends poleward in several areas of the southern Pacific and Indian Oceans. The mean value and standard deviation (shown in Table 1) of the observed February 1998 CLW radiation over tropical oceans are 291.6 and 7.4 W m^{-2}, respectively. Relative to the ERBE February climatological mean CLW field, the February 1998 ENSO event created a large positive anomaly over the entire northern Pacific Ocean. This positive anomaly stretched westward into the Indian Ocean. Areas of positive anomalies are also found in the Southern Hemisphere off the west coast of Africa, South America, and Australia. Negative anomalies occur mainly over areas in the equatorial Pacific and regions of the southeastern Pacific. In addition, negative anomalies are also found in the areas east of the African continent and China. The magnitude of these CLW anomalies ranges between -21 and $+25$ W m^{-2}. Most of the CLW anomalies in the figure fall within ± 9 W m^{-2}. The mean value and standard deviation (shown in Table 1) for the observed February 1998 CLW anomaly over tropical oceans are 2.2 and 4.7 W m^{-2}, respectively.

b. Comparison of observations with model simulations

The observed CERES ERBE-like CLW data were examined to determine their theoretical consistency with the underlying physical state of the atmosphere using radiative transfer model simulation. Comparisons are focused on two specific topics: 1) the spatial distribution of CLW and CLW anomaly fields for February 1998, and 2) the temporal evolution of the CLW radiation field during the first 7 months of 1998.

1) Simulated CLW and CLW anomaly fields

Figure 3c shows the simulated CLW energy field for February 1998 derived from the Fu–Liou radiation model with NOAA SST and NOAA/NCEP data. Despite a small global mean difference of -4.0 W m^{-2} between the simulation and the observations, which is still well within the modeling and observational uncertainties outlined in the earlier sections, the model reproduces the major features/patterns of the observed CLW energy field very realistically. The Northern Hemispheric max-

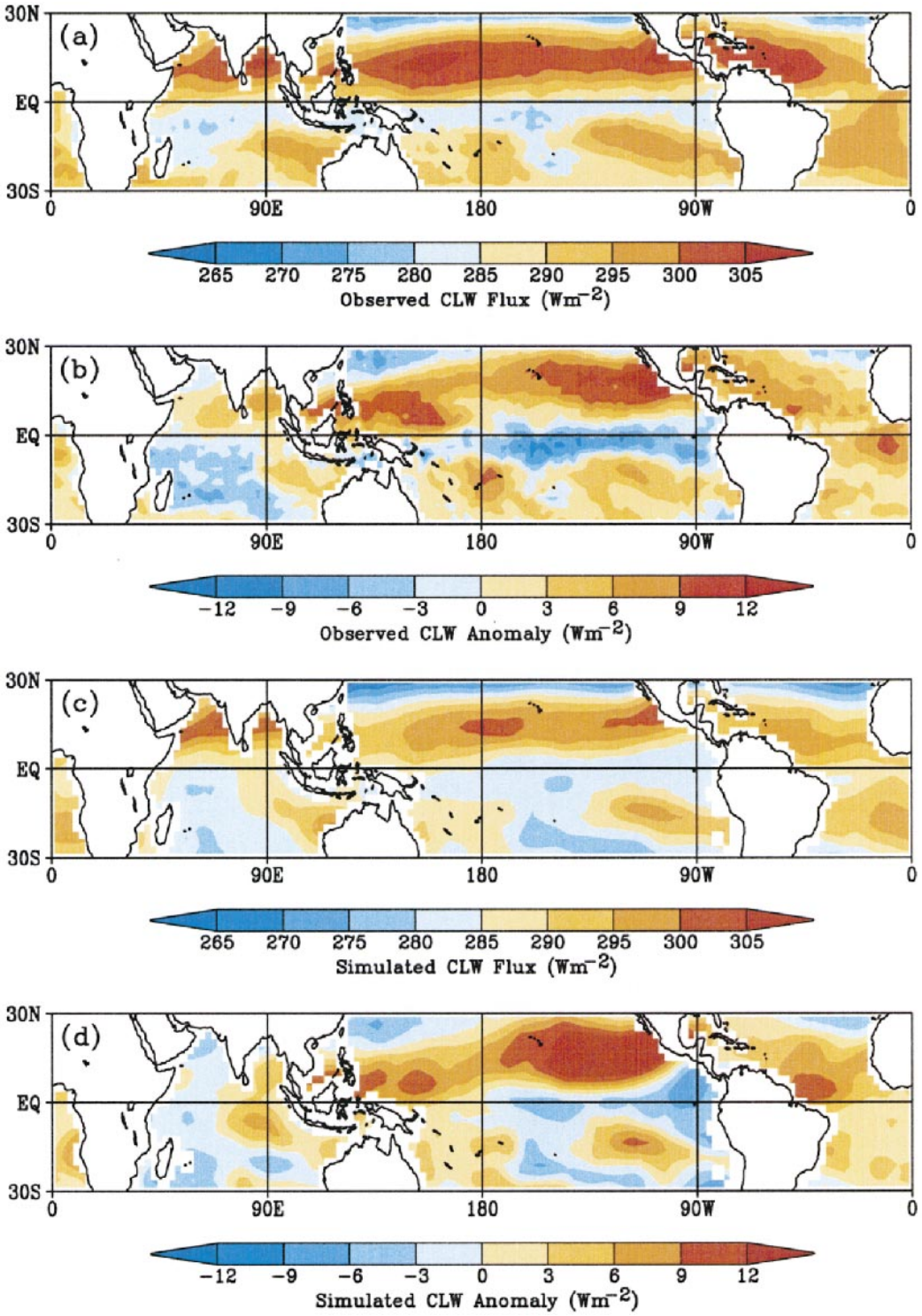

FIG. 3. Spatial distribution of (a) observed oceanic CERES/TRMM ERBE-like CLW field, (b) observed oceanic CERES/TRMM ERBE-like CLW anomaly field, (c) simulated oceanic CLW field, and (d) simulated oceanic CLW anomaly field for Feb 1998.

TABLE 1. Statistical summary (W m^{-2}) of the observed CERES/TRMM ERBE-like and model-simulated Feb 1998 CLW and CLW anomaly fields over oceanic regions between 30°N and 30°S latitude.

	CLW		CLW anomaly	
	Mean	Std dev	Mean	Std dev
CERES	291.6	7.4	2.2	4.7
Model	287.6	7.0	2.3	5.2

imum, the equatorial minimum, the secondary maximum in the Southern Hemisphere, the warm areas west of the major Southern Hemispheric continents, and the northwestward tilt of the warm center west of the Australian continent are all well simulated by the radiative transfer model. In addition, the model also reproduces the distribution of the observed data very well with a simulated standard deviation (shown in Table 1) of 7.0 W m^{-2}. The spatial patterns in this CLW simulation are also highly correlated with the actual ERBE-like observations with a linear correlation coefficient, *R,* of 0.88. Figure 4a presents a comparison between the observed and the simulated tropical oceanic zonal profile of CLW radiation. The small mean difference between the simulated data and the observations shows up clearly in this figure. The source for this discrepancy between model simulation and observations may be caused by a combination of 1) deficiencies in the model physics and inputs used in the simulation and 2) uncertainties in the measurements as discussed in earlier sections. The magnitude of this mean difference also minimizes at the equator and increases poleward away from the equator. These features suggest that the upper-level humidity profile in the McClatchey tropical atmosphere used in our simulation may be too moist, especially in the subtropical subsidence regions near 15°N, and the net effect of these extra moistures is a decrease in the simulated clear-sky outgoing longwave radiation field. In order to further improve the results of the simulation, reliable observations of the upper-level moisture profile are needed. These observations, however, are not currently available. Despite this small disagreement, the similarity between the observed and the simulated zonal profile is quite good. The major maximum in the Northern Hemisphere, the equatorial minimum, and the secondary maximum in the Southern Hemisphere all appear in the correct zonal locations. In addition, the shape of the two profiles follows very closely with each other.

The model-simulated CLW anomaly field for February 1998 is given in Fig. 3d. Despite minor disagreements, the model reproduces the observed CLW anomaly field for February 1998 very well. The large positive anomaly over the entire northern Pacific Ocean, the northwestward tilt of the positive anomaly off the west coasts of Australia and South America, the equatorial negative anomaly, the southeastern Pacific negative anomaly, and the negative anomaly off the east coast of Africa are all well simulated by the model. Minor

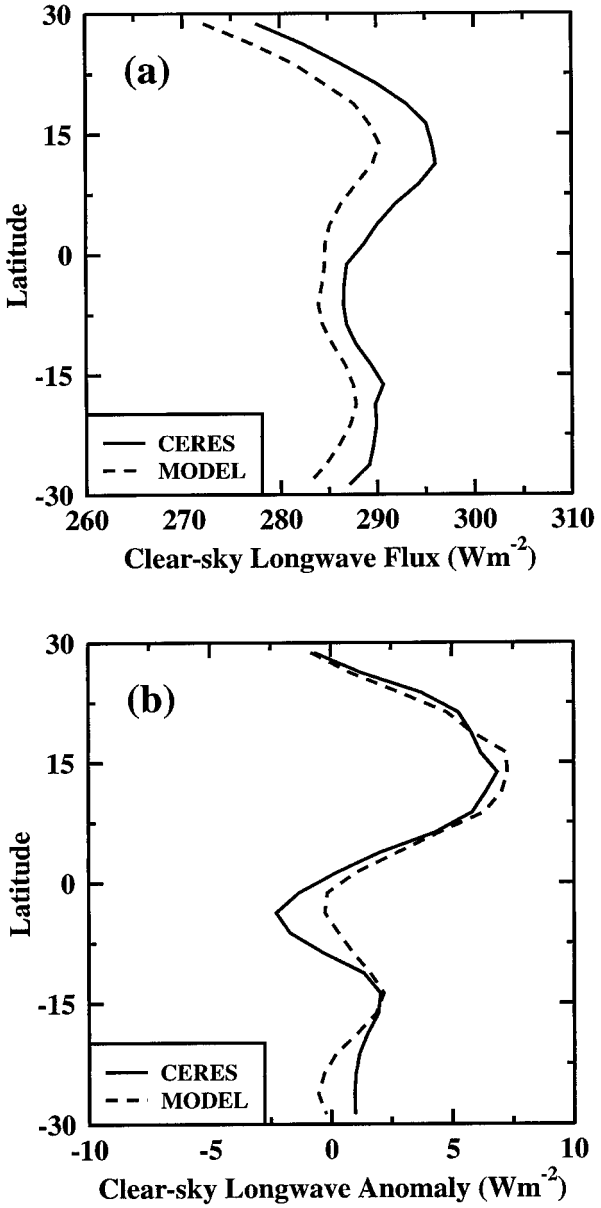

FIG. 4. Observed CERES/TRMM (solid line) and simulated (dashed line) zonal mean profile of oceanic (a) CLW radiation and (b) CLW anomaly field for Feb 1998.

disagreements do occur. For example, the model shows a negative anomaly off the west coast of India while observations reveal a positive anomaly in that region. Equatorial negative anomalies are also less pronounced in the simulated data than in the observed data. In addition, northern Pacific simulations produce larger positive anomalies than that found in observations. Relative to the observed CLW anomaly, the model produces a very similar anomaly (shown in Table 1) with a mean value of 2.3 W m^{-2}. The distribution of the simulated data is slightly larger than those of the observations with a standard deviation of 5.2 W m^{-2}. The spatial corre-

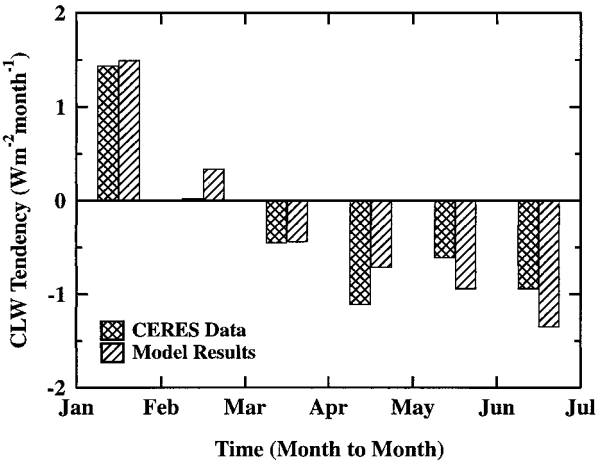

FIG. 5. Time series of monthly tendency of observed CERES/TRMM (gridded pattern) and simulated (shaded pattern) clear-sky longwave oceanic tropical mean value during the first 7 months of 1998.

lation coefficient, *R*, between the simulated anomalies and observations is 0.73. Figure 4b shows the comparison between the zonal mean profile of the simulated and the observed CLW anomaly field over the tropical oceans. The agreement between the two profiles is evident in this figure. In contrast to the clear-sky longwave zonal profile shown in Fig. 4a, the clear-sky longwave anomaly zonal profile shows no systematic differences between observation and simulation. This feature suggests that the February 1998 clear-sky longwave anomaly profile is not very sensitive to deficiencies: 1) imbedded in the radiative transfer simulation and/or 2) related to uncertainties in the observations. In addition, it also hints that the clear-sky longwave anomaly profile is not very perceptive to our treatment of the upper-level humidity profile in the simulations.

2) TEMPORAL EVOLUTION OF THE SIMULATED CLW FIELD

In the previous sections, the spatial distributions of the CLW radiation field and their associated anomaly field from ERBE climatology for February 1998 were analyzed and compared with theoretical simulations. This section concentrates on the temporal evolution of the CLW radiation over tropical oceans during the first 7 months of 1998 as observed by the CERES instrument on the TRMM platform. Specifically, the observed time series of the tropical mean oceanic CLW radiation field between 20°N and 20°S latitude is compared with those produced by radiative transfer model simulation. The results for both the observations and simulations are shown in Fig. 5 in a bar chart representing the monthly tendency of the tropical mean oceanic CLW radiation over the first 7 months of 1998. The observations are reported in gridded pattern and the model results are outlined in shaded pattern. The monthly tendency is defined as the change in oceanic tropical mean CLW value between two consecutive months. The advantage of using this variable is that it allows us to remove the effects of the small bias between the observations and the simulated results as noted in the last section and concentrate on the main features of the two time series. According to this figure, the tendency of the observed tropical oceanic mean CLW radiation field is positive between January and March of 1998. The tendency begins to take a negative turn after March and remains negative for the rest of the data period. The results of the intercomparison between observed and simulated monthly tendency of tropical mean CLW radiation are very good. While small disagreements in the magnitude of the monthly CLW tendency do exist between observations and simulations, the general features and the sign of the simulated monthly CLW tendency match the CERES ERBE-like data very well. These excellent spatial and temporal agreements between the observation and simulation shown in this and previous sections indicate that the CERES ERBE-like CLW observations are theoretically consistent with the underlying surface and atmospheric conditions associated with the 1998 ENSO event.

5. CERES data application study

The 1998 ENSO event is one of the strongest climate anomalies of the twentieth century. The large amount of information collected for this ENSO event makes it an excellent case study. This section describes a CERES data application study that uses the 1998 ENSO event as a natural test bed for understanding physical processes of our climate system. This study takes advantage of the anomaly conditions produced by this ENSO event to examine the physical relationship among changes in SST, PWC, and CLW field and to express the observed ENSO CLW anomaly in terms of fundamental ENSO changes in SST and PWC. An ENSO event is typically marked by a large-scale east–west displacement of elevated SST's over the tropical Pacific Ocean. This east–west migration of the SST pattern, in turn, sets up a chain reaction in the atmosphere that ultimately results in changes in the hydrological cycle (i.e., PWC field) of the tropical Pacific. Since outgoing clear-sky radiation over the ocean is strongly coupled with both the SST and the PWC of the atmosphere (Hallberg and Inamdar 1993; Raval et al. 1994; Collins and Inamdar 1995), changes in these two variables during an ENSO event can directly be translated into changes in outgoing CLW radiation at the TOA. While the change in CLW is positively related to changes in SST, it is negatively associated with changes in PWC. In addition to these direct forcings, SST can also indirectly affect CLW by modifying the PWC field. This indirect forcing, however, is not explicitly explored in this study. A schematic figure of these relationships is outlined in Fig. 6. In order to explore the relative importance of these two

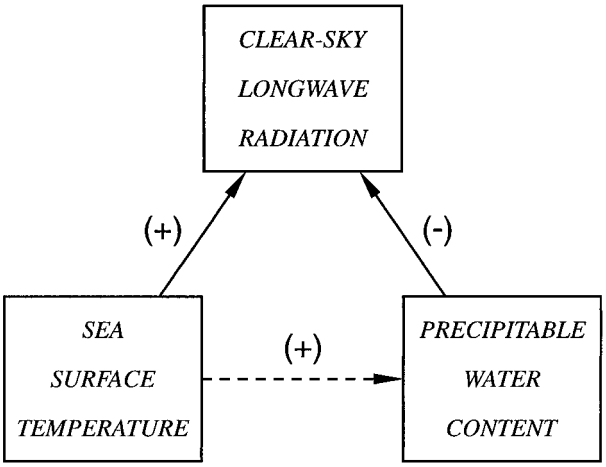

FIG. 6. A schematic figure showing the relationship among SST, PWC, and CLW radiation. Positive (negative) theoretical relationship is indicated by the plus (negative) sign, respectively. Solid line represents direct forcing and dashed line gives indirect forcing.

variables on the outgoing CLW radiation field during the 1998 ENSO event, data analyses are performed using CERES ERBE-like and ERBE observations and NOAA measurements of PWC and SST. The results of these analyses are given below. This information can also be very useful in validating the performance of the general circulation models (GCMs) during the recent ENSO event.

a. Effects of SST anomalies on CLW departures during the 1998 ENSO event

Figures 7a and 7b give the regional pictures of both CLW and the SST anomaly during the January 1998 ENSO event. The SST anomaly field shows the classic ENSO signal with positive anomaly confirmed at the equator, starting just east of the date line and extending eastward to the west coast of America. Smaller negative anomalies are found to the north and south of this large positive ENSO anomaly. This positive SST anomaly, however, does not directly translate into positive changes in CLW field. In contrast, a negative CLW anomaly exists over much of the equatorial Pacific Ocean. Figure 8a shows a scatter diagram of CLW anomaly versus SST anomaly for January 1998 based on the 2.5° resolution datasets. The SST anomaly field for the January 1998 ENSO event is very poorly correlated to the CLW anomaly (i.e., R value of -0.26). The points on the figure are basically clustered at the center of the diagram. We have also reproduced the same scatter diagram using the model-simulated dataset. The results (not shown) are identical to those shown in Fig. 8a. This poor correlation between observed SST anomaly and CLW anomaly over the tropical oceans, as we will see in the next segment, is due to the effect of water vapor absorption in decoupling the surface outgoing CLW energy from the TOA counterpart.

b. Impact of PWC anomaly on CLW departures during the 1998 ENSO event

The PWC anomaly field for the January 1998 ENSO event displayed in Fig. 7c clearly shows the effects of the January 1998 ENSO anomaly in altering the general circulation pattern over the tropical Pacific. Specifically the eastward motion of the warm SST during ENSO had major consequences on both the Walker and Hadley circulations over the tropical ocean. First, it altered the major locations of the Walker circulation in the Pacific. This can been seen by the positive PWC anomaly over the equatorial eastern Pacific and the negative PWC anomaly over the equatorial western Pacific. Second, it created enhanced return flow of the Hadley circulation over the eastern Pacific as seen by the negative anomalies just to the north and south of the major equatorial positive anomaly. These observed ENSO-related PWC features and their inferred general circulation patterns are consistent with published results in the literature. For example, using atmospheric water vapor data produced from the *Nimbus-7* microwave radiometer, Prabhakara et al. 1985 found a similar relationship between the general circulation pattern and the water vapor field during the 1982–1983 ENSO event. Unlike the effects of SST anomaly shown in Fig. 7b, the changes in the PWC field during the January 1998 ENSO event can be clearly seen as having a negative effect in the outgoing CLW anomaly field at TOA. For example, the major positive PWC anomalies in Fig. 7c over the equatorial eastern Pacific and east of Africa show up clearly as a negative anomaly in the CLW field in Fig. 7a. The negative PWC anomalies that stretch from west of Australia northeastward into the equatorial western Pacific and continue northeastward across into the northern equatorial eastern Pacific are also translated into positive CLW anomalies over those areas. The northeastward tilt of the CLW anomalies correlate very well with the same feature in the PWC anomaly field. Figure 8b gives a scatter diagram of these two variables. The negative relationship between the PWC anomaly and the CLW anomaly clearly shows up as a negative slope in this figure. A least squares fit to the data has a negative slope of -0.57 and an intercept of 1.51. The linear correlation coefficient, R, between the PWC anomaly and the CLW anomaly is -0.63. This again points to the significant influence of water vapor in modulating the outgoing CLW radiation over the tropical atmosphere during the January 1998 ENSO event. In the moist tropical atmosphere, the longwave energy emitted from the surface is mostly absorbed by the water vapor in the atmosphere. This radiation is reemitted back to the atmosphere. The level at which the reemission occurs is dependent on the column water vapor content. When the atmosphere is drier, longwave energy is able to escape from the lower troposphere to the TOA and the net effect is an increase in outgoing CLW radiation at the TOA. As the moisture content of the atmosphere increases, the effective longwave emission level in the atmosphere moves upward, away from the surface and the net effect is a

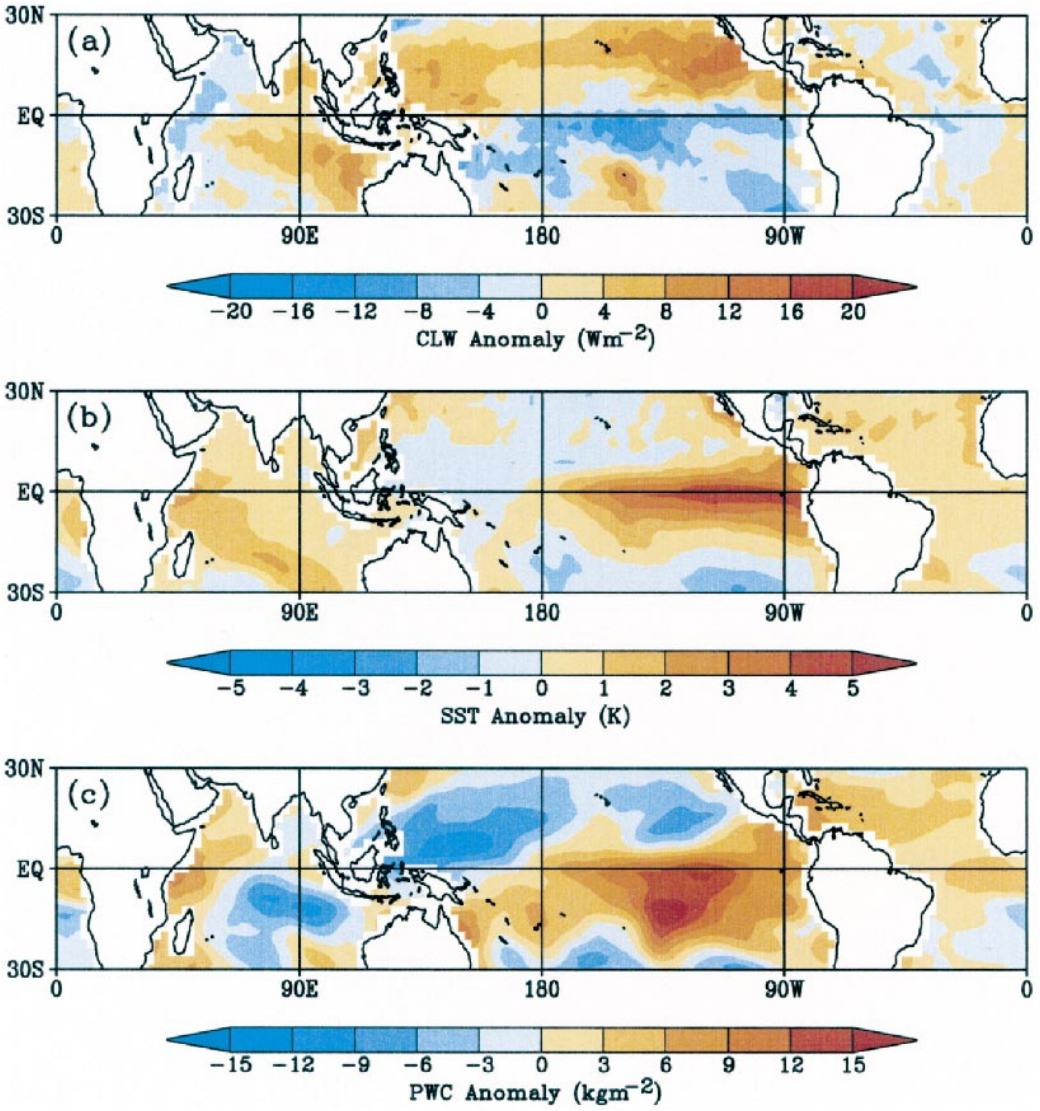

FIG. 7. Spatial distribution of observed oceanic (a) CERES/TRMM ERBE-like CLW anomaly field, (b) NOAA SST anomaly field, and (c) NOAA PWC anomaly field during Jan 1998.

decrease in outgoing longwave radiation at TOA. These observed relationships between changes in SST, PWC, and CLW over the tropical ocean during the 1998 ENSO event are consistent with the known SST–PWC–CLW relationship found in the scientific literature (i.e., Hallberg and Inamdar 1993; Raval et al. 1994; Collins and Inamdar 1995) and again point to the important role of water vapor absorption in decoupling the outgoing surface CLW energy field from its TOA counterpart. In terms of a climate feedback mechanism, an increase in water vapor increases the greenhouse effect by reducing the CLW, thus acting as a positive climate feedback.

6. Summary and conclusions

This paper presents the initial postlaunch validation for the clear-sky longwave component of the CERES/TRMM edition-1 ERBE-like monthly mean data product. The validation approach involves a combination of CERES and ERBE observations and model simulations using the Fu–Liou radiative transfer model. Observational analyses of the observed CLW are performed for the first 7 months of 1998. An ENSO-like feature is found in the time series of CLW field. This feature has a peak value during February, corresponding to the peak of the 1998 ENSO event. Due to this ENSO event, the CERES ERBE-like CLW observations are also found to be outside the maximum range of the ERBE climatology during the six of the seven months that have been examined. The ERBE-like CLW finally matches the ERBE climatology as the 1998 ENSO event came to a conclusion in July 1998. In order to check for theoretical consistency of the new ERBE-like CLW dataset, comparisons are performed between observations and ra-

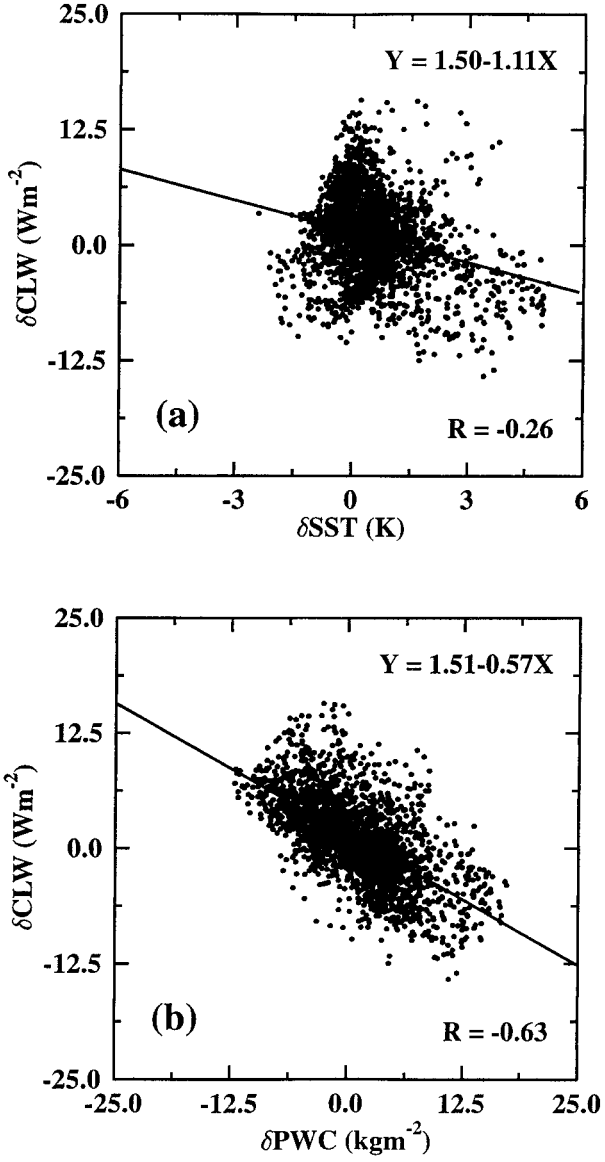

FIG. 8. Scatter diagram of observed oceanic (a) NOAA SST anomaly field versus CERES/TRMM ERBE-like CLW anomaly field and (b) NOAA PWC anomaly field versus CERES/TRMM ERBE-like CLW anomaly field for Jan 1998.

diation transfer simulations. In general, the simulated CLW and CLW anomaly fields for February 1998 are consistent with those obtained from observations. Although the model simulations have a small bias, the spatial distribution of the February 1998 CLW radiation simulation and the CLW anomaly simulations matched very well with the actual spatial distribution of the observations. In addition, the temporal evolution of the tropical mean CLW tendency during the 1998 ENSO events from January to July is well captured by the model simulations using observed sea surface temperature and temperature and moisture profiles of the atmosphere. The excellent spatial and temporal agreements between observations and simulations shown in this validation study indicate that the CERES ERBE-like CLW observations are theoretically consistent with the underlying surface and atmospheric conditions associated with the 1998 ENSO event.

This paper also describes a CERES data application study that demonstrates the scientific benefit of this new dataset. Using the January 1998 ENSO event as a natural test bed for understanding physical processes of our climate system, this paper sets out to examine the physical relationship between changes in SST, PWC, and CLW field during the 1998 ENSO event. The information gathered from this study can also be very useful in validating the performance of the GCMs during the 1998 ENSO event. Outgoing CLW radiations over the ocean can be influenced by both the SST and the PWC of the atmosphere. Changes in these two variables during the ENSO event can directly be translated into changes in outgoing CLW radiation at TOA. While the change in CLW is positively related to changes in SST, it is negatively associated with changes in PWC. While an inverse relationship is observed between the CLW anomaly and the PWC anomaly for the January 1998 ENSO event, very little direct correlation is found between the CLW anomaly and SST anomaly. These observed features in the CLW energy field are consistent with the physics of the tropical atmosphere, where the large water vapor absorption in the atmosphere can effectively decouple the surface upward longwave radiation field from its corresponding TOA counterpart. These results agree well with findings from previous studies and again point to the significance of the water vapor, an important atmospheric greenhouse gas, in modulating the TOA distribution of tropical oceanic CLW radiation.

Following the legacy of the ERBE measurements, the new CERES ERBE-like observations will continue to provide a fundamental climate dataset for researchers worldwide to examine climate issues and to study the TOA radiative energy budget of the earth–atmosphere systems. In addition to its vital long-term climate monitoring capability, this dataset can also be used to improve performance and prediction of the global general circulation models and to advance our current understanding on the physical links and feedback processes between various meteorological and climatic parameters and the TOA radiative energy field. The CERES/TRMM edition-1 ERBE-like dataset is currently available at the NASA Langley DAAC. The Langley DAAC can be reached through the World Wide Web at http://eosweb.larc.nasa.gov/.

Acknowledgments. This research was supported by the NASA Earth Observing System Interdisciplinary Program, NASA Office of Earth Sciences through the CERES Project, and the NASA Langley Research Center under Grants NCC-1-243 and NAG-1-2106. The authors would like to acknowledge the NASA Langley

DAAC for providing the CERES and ERBE datasets, NOAA/NCEP for furnishing the Reynolds SST and atmospheric datasets, and NOAA/CDC for supplying the ENSO index. In addition, we would also like to thank Dr. David Kratz (NASA LaRC) for performing the line-by-line calculations, Dr. Norman Loeb (Hampton University) for discussion on Longwave ADM, and Dr. Bruce Wielicki (NASA LaRC) for many hours of interesting discussion. Finally, we would like to acknowledge the two anonymous journal reviewers for their constructive comments.

REFERENCES

Barkstrom, B. R., 1984: The Earth Radiation Budget Experiment (ERBE). *Bull. Amer. Meteor. Soc.,* **65,** 1170–1185.

——, E. F. Harrison, G. L. Smith, R. N. Green, J. Kibler, R. D. Cess, and the ERBE Science Team, 1989: Earth Radiation Budget Experiment (ERBE) archival and April 1985 results. *Bull. Amer. Meteor. Soc.,* **70,** 1254–1262.

Brooks, D. R., E. F. Harrison, P. Minnis, J. T. Suttles, and R. S. Kandel, 1986: Development of algorithms for understanding the temporal and spatial variability of the earth's radiation balance. *Rev. Geophys.,* **24,** 422–438.

Charlock, T. P., and T. L. Alberta, 1996: The CERES/ARM/GEWEX Experiment (CAGEX) for the retrieval of radiative fluxes with satellite data. *Bull. Amer. Meteor. Soc.,* **77,** 2673–2683.

——, and Coauthors, 1995: Compute surface and atmospheric fluxes (Subsystem 5.0). *Clouds and the Earth's Radiant Energy System (CERES) Algorithm Theoretical Basis Document, Volume IV: Determination of Surface and Atmosphere Fluxes and Temporally and Spatially Averaged Products (Subsystems 5–12),* NASA RP-1376, CERES Science Team, Eds., NASA Langley Research Center, 1–51.

Collins, W. D., and A. K. Inamdar, 1995: Validation of clear-sky fluxes for tropical oceans from the Earth Radiation Budget Experiment. *J. Climate,* **8,** 569–578.

Fu, Q., and K.-N. Liou, 1992: On the correlated *k*-distribution method for radiative transfer in nonhomogeneous atmospheres. *J. Atmos. Sci.,* **49,** 2139–2156.

——, and ——, 1993: Parameterization of the radiative properties of cirrus clouds. *J. Atmos. Sci.,* **50,** 2008–2025.

Hallberg, R., and A. K. Inamdar, 1993: observations of seasonal variations in atmospheric greenhouse trapping and its enhancement at high sea surface temperature. *J. Climate,* **6,** 920–931.

Harrison, E. F., P. Minnis, B. R. Barkstrom, V. Ramanathan, R. D. Cess, and G. G. Gibson, 1990: Seasonal variation of cloud radiative forcing derived from the Earth Radiation Budget Experiment. *J. Geophys. Res.,* **95,** 18 687–18 703.

Hartmann, D. L., and D. Doelling, 1991: On the net radiative effectiveness of clouds. *J. Geophys. Res.,* **96,** 869–891.

——, M. E. Ockert-Bell, and M. L. Michelsen, 1992: The effect of cloud type on earth's energy balance: Global analysis. *J. Climate,* **5,** 1281–1304.

Kiehl, J. T., and B. P. Briegleb, 1992: Comparison of the observed and calculated clear-sky greenhouse effect: Implications for climate studies. *J. Geophys. Res.,* **97,** 10 037–10 049.

McClatchey, R. A., R. W. Fenn, J. E. A. Selby, F. E. Volz, and J. S. Garing, 1972: Optical properties of the atmosphere. Environmental Research Paper 411, Air Force Cambridge Research Laboratory, Bedford, Massachusetts, 108 pp. [Available from AFCRL, Bedford, MA 01730.]

Ockert-Bell, M. E., and D. L. Hartmann, 1992: The effect of cloud type on earth's energy balance: Results for selected regions. *J. Climate,* **5,** 1157–1171.

Prabhakara, C., D. A. Short, and B. E. Vollmer, 1985: El Niño and atmospheric water vapor: Observations from Nimbus 7 SMMR. *J. Climate Appl. Meteor.,* **24,** 1311–1324.

Raval, A., A. H. Oort, and V. Ramaswamy, 1994: Observed dependence of outgoing longwave radiation on sea surface temperature and moisture. *J. Climate,* **7,** 807–821.

Simpson, J., R. F. Adler, and G. R. North, 1988: A proposed Tropical Rainfall Measuring Mission (TRMM) satellite. *Bull. Amer. Meteor. Soc.,* **69,** 278–295.

Suttles, J. T., and Coauthors, 1988: *Angular Radiation Models for Earth–Atmosphere System.* Vol. I, *Shortwave Radiation.* NASA RP-1184, NASA Langley Research Center, 144 pp.

Wielicki, B. A., and R. N. Green, 1989: Cloud identification for ERBE radiative flux retrieval. *J. Appl. Meteor.,* **28,** 1133–1146.

——, R. D. Cess, M. D. King, D. A. Randall, and E. F. Harrison, 1995: Mission to Planet Earth: Role of clouds and radiation in climate. *Bull. Amer. Meteor. Soc.,* **76,** 2125–2153.

——, B. R. Barkstrom, E. F. Harrison, R. B. Lee III, G. L. Smith, and J. E. Cooper, 1996: Clouds and the Earth's Radiant Energy System (CERES): An Earth Observing System experiment. *Bull. Amer. Meteor. Soc.,* **77,** 853–868.

——, and Coauthors, 1998: Clouds and the Earth's Radiant Energy System (CERES): Algorithm overview. *IEEE Trans. Geosci. Remote Sens.,* **36,** 1127–1141.

Wolter, K., and M. S. Timlin, 1993: Monitoring ENSO in COADS with a seasonally adjusted principal component index. *Proc. 17th Climate Diagnostics Workshop,* Norman, OK, NOAA/NMC/CAC, NSSL, Oklahoma Climate Survey, CIMMS and the School of Meteorology, University of Oklahoma, 52–57.

——, and ——, 1998: Measuring the strength of ENSO—How does 1997/98 rank? *Weather,* **53,** 315–324.

Young, D. F., P. Minnis, D. R. Doelling, G. G. Gibson, and T. Wong, 1998: Temporal interpolation methods for the Clouds and the Earth's Radiant Energy System (CERES) experiment. *J. Appl. Meteor.,* **37,** 572–590.